FINITE DIFFERENCE SYNTHETIC ACOUSTIC LOGS

R.A. Stephen*, F. Pardo-Casas and C.H. Cheng

Earth Resources Laboratory
Department of Earth and Planetary Sciences
Massachusetts Institute of Technology
Cambridge, MA 02139

ABSTRACT

Synthetic seismograms of elastic wave propagation in a fluid-filled borehole were generated using both the finite difference technique and the discrete wavenumber summation technique. The latter is known to be accurate for both body and surface (guided) waves. The finite difference grid has absorbing boundaries on two sides and axes of symmetry on the remaining two sides. A grid size no less than 10 points per wavelength was used. The far absorbing boundary was located at a distance of five to 10 radii from the borehole. Two types of solid-liquid interfaces were investigated: 1) a velocity gradient using the heterogeneous formulation, and 2) a sharp boundary using a second order Taylor expansion of the displacements. The results from the finite difference modeling were compared with the synthetic seismograms generated by the discrete wavenumber summation method. No comparison the heterogeneous formulation and the discrete wavenumber method has been made. The second order approximation to the solid-liquid interface produced seismograms that compared well with the discrete wavenumber seismograms. A detailed comparison between the seismograms generated by the two methods showed that the body waves (refracted P and S waves) are identical, while the guided waves showed a slight difference in both phase and amplitude. These differences are believed to be due to the approximations introduced in the fluid-solid interface, the absorbing boundary at the edge of the grid, and the grid and time step sizes involved. Owing to the fact that they are interface waves, the guided waves, especially the higher modes, are much more sensitive to the above mentioned approximations.

INTRODUCTION

In order to obtain the best possible interpretation of an acoustic log it is necessary to fully understand the physics of acoustic and elastic wave propagation in and around the borehole. Because of the complexity of the wave equations involved, models of the acoustic logging problem almost always assume radial symmetry and depth independent elastic properties (e.g., Biot, 1952; White and Zechman, 1968; Tsang and Rader, 1979; Cheng and Toksöz, 1981). This type of analysis is certainly acceptable for identifying the major

---

*permanent address: P.O.Box 567, West Falmouth, MA 02574

modes of wave propagation and their ideal properties. The next step in studying the problem is to gain some insight into the effects of more realistic structure. How does variable borehole diameter between the source and receiver affect the logs? How would thin layers and horizontal bed boundaries change the observed waveforms? At the present time only finite difference or finite element methods applied to the elastic wave equation have the potential to answer these questions. Stephen (1983) had applied finite difference methods to seismic wave propagation through the sea floor. This is a theoretically similar problem to seismic wave propagation in a borehole. For this reason, the finite difference method was chosen to address some of the above mentioned problems.

The first task is to compare finite difference acoustic logs with logs generated by the discrete wave number approach (Cheng and Toksöz, 1981). This will provide a useful check on the accuracy of the two methods since they are fundamentally different ways of solving the same problem and the nature of the numerical approximations in each case is entirely different. This paper will outline the finite difference method as applied to the acoustic logging problem, as well as report the preliminary findings of the comparison between the results of the finite difference and discrete wavenumber analysis.

THE FINITE DIFFERENCE METHOD

A list of all the papers on the finite difference method in seismology would be too lengthy to include here. Three groups were "pioneers" in the work (see for example Alterman and Karal (1968); Boore (1972); Kelly *et. al.* (1976)). Stephen (1983) has given finite difference formulations for sharp liquid-solid interfaces and compared the results to the reflectivity method (a discrete wave number technique) for sea floor models.

The equation to be solved is the elastic wave equation for perfectly elastic, isotropic media in the absence of body forces (Aki and Richards, 1980):

$$\rho \ddot{u}_i = \tau_{ij,j} \tag{1}$$

where ρ is density, u_i is the displacement vector and τ_{ij} is the stress tensor for isotropic media, with summation over repeated indices. Anisotropy and attenuation can be included in the finite difference solution if necessary. The stress tensor for isotropic media can be written as

$$\tau_{ij} = [\lambda \delta_{ij} \delta_{kl} + \mu(\delta_{ik}\delta_{jl} + \delta_{il}\delta_{jk})]e_{kl} \tag{2}$$

where λ and μ are Lame's parameters, δ_{ij} is the Kronecker delta, and $e_{kl} = \frac{1}{2}(u_{k,l} + u_{l,k})$ is the strain tensor. Equation (1) will be solved in two-dimensional cylindrical co-ordinates (r,z) and the parameters (ρ,λ,μ) will be assumed to be functions of radius r and depth z only. A purely compressional source will be located in a liquid on the axis of symmetry ($r=0$) and a liquid-solid interface will be located at a radius, R. A vertical line of pressure receivers will be located below the source on the axis of symmetry (Figure 1).

The time dependence of the potential of the impulsive compressional point source is given by Kelly *et al.* (1976):

$$f(t) = -2\xi(t - t_s)e^{-\xi(t-t_s)^2} \tag{3}$$

where t_s is a time shift chosen such that $f(0) \approx 0$ and ξ governs the pulse width.

Stephen (1983) showed that in order to obtain agreement between finite difference and discrete wavenumber approaches for liquid-solid interfaces, it was necessary in the finite difference method to specifically code the boundary conditions for the sharp interface and that a code correct to second order in the space increments gave the best results. The above mentioned paper dealt with sea floor models. In this paper, the finite difference formulation for slowly varying media will be reviewed and the second-order formulation for a sharp liquid-solid borehole interface will be given.

Formulation for Slowly Varying Media

As outlined by Alterman and Loewenthal (1972) and Kelly *et al.* (1976) the elastic wave equation with the parameters (ρ,λ,μ), functions of range and/or depth can be solved directly by an explicit finite difference method. In terms of displacements only, equations (1) and (2) become

$$\rho\ddot{\vec{u}} = (\lambda+\mu)\nabla(\nabla\cdot\vec{u}) + \mu\nabla^2\vec{u} + \nabla\lambda(\nabla\cdot\vec{u}) + \nabla\mu\times(\nabla\times\vec{u}) + 2(\nabla\mu\cdot\nabla)\vec{u} \tag{4}$$

The finite difference formulation of this equation is given in Stephen (1983). It is important to note that there are a number of explicit finite difference formulations for this equation and stability and accuracy will differ for each one (Zienkiewicz, 1977). Thus it is important to state precisely which formulation is used in a particular application. It is necessary to allow for density variations in the code because of the sharp density contrast at the borehole wall. The borehole fluid can be considered simply by letting the shear modulus, μ, go to zero.

For the case of propagation in infinite homogeneous media, this explicit finite difference formulation is stable only if:

$$\Delta t \leq \frac{\min(\Delta r, \Delta z)}{\sqrt{\alpha^2+\beta^2}} \tag{5}$$

where $\alpha = \sqrt{\frac{\lambda+2\mu}{\rho}}$, and $\beta = \sqrt{\frac{\mu}{\rho}}$. Kelly *et al.* (1976) suggested that stability in heterogeneous media could be expected provided equation (5) held everywhere on the grid. Experience suggests that this is only the case for "slowly" varying media.

The principle cause of inaccuracy in finite difference calculations for slowly varying media is grid dispersion. If the grid increments $(\Delta r, \Delta z)$ are too large, low frequencies will travel faster across the grid than high frequencies causing apparent dispersion. (This result is generally true for compressional waves. For shear waves the dispersion relation is more complex and for some combinations of Poisson's ratio and propagation direction high frequencies will travel faster than low frequencies (see Bamberger *et al.* (1980)). Estimates of

the number of grid points per wavelength which will give acceptable results vary from ten to fifty and depend on the problem. This uncertainty makes the comparison of finite difference results with results of other techniques extremely important.

Second Order Boundary Conditions for a Liquid-Solid Cylindrical Interface

Stephen (1983) showed that it is necessary to represent the liquid-solid interface specifically in the finite difference code by boundary conditions. Unfortunately the formulation given by Stephen (1983) was for interfaces normal to the depth z axis and is inappropriate for interfaces normal to the radius r in cylindrical co-ordinates. The formulation for this case, which is analogous to a formulation for solid-solid interfaces originally presented by Ungar and Ilan (1977) is given below.

The wave equation in the homogeneous liquid to the left of the interface (see Figure 1) is:

$$\rho_1 u_{tt}^1 - \lambda_1 (u_{rr}^1 + \frac{1}{r} u_r^1 - \frac{1}{r^2} u^1) - \lambda_1 w_{rz}^1 = 0 \tag{6}$$

$$\rho_1 w_{tt}^1 - \lambda_1 (u_{rz}^1 + \frac{1}{r} u_z^1) - \lambda_1 w_{zz}^1 = 0 \tag{7}$$

and in the homogeneous solid to the right of the interface is:

$$\rho_2 u_{tt}^2 - (\lambda_2+\mu_2)(u_{rr}^2 + \frac{1}{r} u_r^2 - \frac{1}{r^2} u^2) - \mu_2 u_{zz}^2 - (\lambda_2+\mu_2) w_{rz}^2 = 0 \tag{8}$$

$$\rho_2 w_{tt}^2 - \mu_2 (w_{rr}^2 + \frac{1}{r} w_r^2) - (\lambda_2+2\mu_2) w_{zz}^2 - (\lambda_2+\mu_2)(u_{rz}^2 + \frac{1}{r} u_z^2) = 0 \tag{9}$$

The boundary conditions which must hold at the liquid-solid interface are continuity of normal stress,

$$\lambda_1 (u_r^1 + \frac{1}{r} u^1) + \lambda_1 w_z^1 = (\lambda_2+2\mu_2) u_r^2 + \lambda_2 (\frac{1}{r} u^2 + w_z^2) \tag{10}$$

vanishing of the tangential stress in the solid,

$$\mu_2 (u_z^2 + w_r^2) = 0 \tag{11}$$

and continuity of normal displacement,

$$u^1 = u^2 \tag{12}$$

The superscripts, 1 and 2, refer to values in the liquid and solid respectively. The unknowns in the derivation are the horizontal displacement at the interface, $u^{1,2}(M,n,l)$, the vertical displacement in the liquid at the interface, $w^1(M,n,l)$ and the vertical displacement in the solid at the interface, $w^2(M,n,l)$. The interface is at a radius of $R=M\Delta r$.

Additional relationships required in the derivation are the Taylor expansions:

$$-\Delta r u_r^1+\frac{1}{2}\Delta r^2 u_{rr}^1=u^1(M-1,n,l)-u^1(M,n,l) \tag{13}$$

$$\Delta r u_r^2+\frac{1}{2}\Delta r^2 u_{rr}^2=u^2(M+1,n,l)-u^2(M,n,l) \tag{14}$$

$$\Delta r w_r^2+\frac{1}{2}\Delta r^2 w_{rr}^2=w^2(M+1,n,l)-w^2(M,n,l) \tag{15}$$

and the finite difference expressions for mixed derivatives:

$$-2\Delta r\,\Delta z w_{rz}^1=w^1(M-1,n+1,l)-w^1(M-1,n-1,l)$$
$$-w^1(M,n+1,l)+w^1(M,n-1,l) \tag{16}$$

$$2\Delta r\,\Delta z u_{rz}^2=u^2(M+1,n+1,l)-u^2(M+1,n-1,l)$$
$$-u^2(M,n+1,l)+u^2(M,n-1,l) \tag{17}$$

$$2\Delta r\,\Delta z w_{rz}^2=w^2(M+1,n+1,l)-w^2(M+1,n-1,l)$$
$$-w^2(M,n+1,l)+w^2(M,n-1,l). \tag{18}$$

The finite difference formulation for the horizontal displacement on the interface, is obtained by solving equations (6), (8), (10), (12), (13), (14), (16) and (18) and replacing z and t derivatives with centered finite differences. Hence:

$$\begin{aligned}
u^{1,2}(M,n,l+1)=&2u^{1,2}(M,n,l)-u^{1,2}(M,n,l-1)\\
&+a_1[w^2(M,n+1,l)-w^2(M,n-1,l)]\\
&+a_2[w^1(M,n+1,l)-w^1(M,n-1,l)]\\
&+a_3u^{1,2}(M,n,l)\\
&+a_4[u^2(M+1,n,l)-u^{1,2}(M,n,l)]\\
&+a_5[u^{1,2}(M,n,l)-u^1(M-1,n,l)]\\
&+a_6[u^{1,2}(M,n+1,l)-2u^{1,2}(M,n,l)+u^{1,2}(M,n-1,l)]\\
&+a_7[w^2(M+1,n+1,l)-w^2(M,n+1,l)-w^2(M+1,n-1,l)+w^2(M,n-1,l)]\\
&+a_8[w^1(M,n+1,l)-w^1(M-1,n+1,l)-w^1(M,n-1,l)+w^1(M-1,n-1,l)]
\end{aligned}$$

where

$$a_1=\frac{\Delta t^2}{\Delta r\Delta z}\frac{\lambda_2}{(\rho_1+\rho_2)}$$

$$a_2=-\frac{\Delta t^2}{\Delta r\Delta z}\frac{\lambda_1}{(\rho_1+\rho_2)}$$

$$a_3=\frac{\Delta t^2}{\Delta r^2}\frac{2}{(\rho_1+\rho_2)}[\frac{1}{M}(\lambda_2-\lambda_1)-\frac{1}{2M^2}(\lambda_2+2\mu_2+\lambda_1)]$$

$$a_4=\frac{\Delta t^2}{\Delta r^2}\frac{2(\lambda_2+2\mu_2)}{(\rho_1+\rho_2)}(1+\frac{1}{2M})$$

$$a_5=-\frac{\Delta t^2}{\Delta r^2}\frac{2\lambda_1}{(\rho_1+\rho_2)}(1-\frac{1}{2M})$$

$$a_6=\frac{\Delta t^2}{\Delta z^2}\frac{\mu_2}{(\rho_1+\rho_2)}$$

$$a_7=\frac{\Delta t^2}{\Delta r\Delta z}\frac{(\lambda_2+\mu_2)}{2(\rho_1+\rho_2)}$$

$$a_8=\frac{\Delta t^2}{\Delta r\Delta z}\frac{\lambda_1}{2(\rho_1+\rho_2)}$$

In all the formulations presented in this paper $\vec{u}=(u,w);\Delta r,\Delta z,\Delta t$ are the increments in radius, depth and time and m, n, l are the indices for radius, depth and time (i.e. $(m,n,l)=(m\Delta r,n\Delta z,l\Delta t)$).

Similarly by solving equations (6), (7) and (13) for the vertical displacement in the liquid at the interface one obtains:

$$\begin{aligned}w^1(M,n,l+1)=&2w^1(M,n,l)-w^1(M,n,l-1)\\&+b_1[w^1(M,n+1,l)-2w^1(M,n,l)+w^1(M,n-1,l)]\\&+b_2[u^1(M,n+1,l)-u^1(M,n-1,l)]\\&+b_3[u^1(M,n+1,l)-u^1(M-1,n+1,l)-u^1(M,n-1,l)+u^1(M-1,n-1,l)]\\&+b_4[u^1(M,n+1,l+1)-2u^1(M,n+1,l)+u^1(M,n+1,l-1)\\&\quad-u^1(M,n-1,l+1)+2u^1(M,n-1,l)-u^1(M,n-1,l-1)]\\&+b_5[w^1(M,n+1,l)-2w^1(M,n,l)+w^1(M,n-1,l)\\&\quad-w^1(M-1,n+1,l)+2w^1(M-1,n,l)-w^1(M-1,n-1,l)]\\&+b_6[u^1(M,n+1,l)-u^1(M,n-1,l)-u^1(M-1,n+1,l)+u^1(M-1,n-1,l)]\end{aligned}$$

where

$$b_1=\left(\frac{\Delta t^2}{\Delta z^2}\right)^2\frac{\lambda_1}{\rho_1}$$

$$b_2=\frac{\Delta t^2}{\Delta r\,\Delta z}\frac{\lambda_1}{2\rho_1}\left(\frac{1}{M}+\frac{1}{2M^2}\right)$$

$$b_3=\frac{\Delta t^2}{\Delta r\,\Delta z}\frac{\lambda_1}{2\rho_1}$$

$$b_4=\frac{\Delta r}{4\Delta z}$$

$$b_5=-\frac{\Delta t^2}{\Delta z^2}\frac{\lambda_1}{2\rho_1}$$

$$b_6=-\frac{\Delta t^2}{\Delta z\,\Delta r}\frac{\lambda_1}{\rho_1}\frac{1}{4M.}$$

Note that this solution requires the horizontal component on the interface at future points in time ($(l+1)\Delta t$) and it must follow the calculation of the horizontal components.

The vertical displacement in the solid at the interface is obtained from equations (9), (11), (15), and (17):

$$\begin{aligned}w^2(M,n,l+1)=&2w^2(M,n,l)-w^2(M,n,l-1)\\&+c_1[u^{1,2}(M,n+1,l)-u^{1,2}(M,n-1,l)]\\&+c_2[w^2(M+1,n,l)-w^2(M,n,l)]\\&+c_3[w^2(M,n+1,l)-2w^2(M,n,l)+w^2(M,n-1,l)]\\&+c_4[u^2(M+1,n+1,l)-u^2(M,n+1,l)-u^2(M+1,n-1,l)+u^2(M,n-1,l)]\end{aligned}$$

where

$$c_1=\frac{\Delta t^2}{\Delta r\,\Delta z}\frac{\mu_2}{\rho_2}\left[1+\frac{1}{2M}\frac{(\lambda_2+\mu_2)}{\mu_2}\right]$$

$$c_2=\frac{\Delta t^2}{\Delta r^2}\frac{2\mu_2}{\rho_2}\left(1+\frac{1}{2M}\right)$$

$$c_3=\frac{\Delta t^2}{\Delta z^2}\left(\frac{\lambda_2+2\mu_2}{\rho_2}\right)$$

$$c_4=\frac{\Delta t^2}{\Delta r\,\Delta z}\left(\frac{\lambda_2+\mu_2}{2\rho_2}\right)$$

Boundary Conditions

In order to minimize the computation time for the problem, it is necessary to minimize the size of the grid. This is accomplished by the proper selection of axes of symmetry and absorbing boundaries. If absorbing boundaries were not used (e.g., the displacement is simply set to zero at some distance from the source), the grid dimensions would be necessarily large in order to prevent the reflections from these artificial boundaries producing interference at the receivers.

In the present model the top and left-hand boundaries are selected to be axes of symmetry, thus placing the compressional point source in the upper left corner. Exact finite difference formulation to the elastic wave equation is possible at axes of symmetry and these are generally preferable to absorbing boundaries where approximations must be made. The axes of symmetry formulations can be obtained from the body formulations outlined in the previous section by either 1) applying symmetry conditions for the displacements (e.g., for the left-hand boundary, vertical displacements are symmetrical on either side of the axis and horizontal displacements are asymmetrical on either side of the axis) or 2) apply l'Hospital's rule for terms containing $\partial / \partial r$, as outlined by Alterman and Loewenthal (1972), (e.g., for the left-hand boundary, $\frac{1}{r}\frac{\partial u}{\partial z}$ becomes $\frac{\partial^2 u}{\partial r \partial z}$ as r goes to zero).

A special code for the absorbing boundaries follows the formulation of Clayton and Engquist (1977), as modified by Emerman and Stephen (1983). The method assumes a parabolic approximation to the elastic wave equation about an axis normal to the boundary and works best for energy propagating at near normal incidence. The absorbing boundary conditions are applied in cylindrical coordinates for the liquid and in cartesian coordinates, assuming $1/r$ small enough, in the solid.

The intersection of the sharp interface and the absorbing boundary(joint point) requires special treatment. For the horizontal displacement and the vertical displacement in the solid the same absorbing boundary formulation as used for heterogeneous media was applied, with the velocities and densities at the point of intersection replaced by the average values across the interface. The vertical displacement in the liquid was computed using a first-order one-sided difference of the equation for the continuity of normal stress. Although not very rigorous, this technique seems to work reasonably well. As pointed out by Fuyuki and Matsumoto (1980), the guided waves are not absorbed by this kind of boundary. Owing to the elliptical particle motion of the guided waves, there is a component of displacement parallel to the boundary which may pose problems if the boundary is close to the borehole. A minimum of two wavelengths of the lowest frequency guided wave was used as a criterion for the placement of the grid boundary from the liquid-solid sharp interface to avoid this problem.

NUMERICAL RESULTS

In this section, preliminary results in applying the heterogeneous and sharp interface formulations outlined above to produce synthetic acoustic logs will be discussed. Problems which did not arise in previous work with finite

difference solutions have been encountered. However, the problems occur late in the wave train, after the Stoneley wave arrivals, and our solutions appear reasonable for the earlier phases.

Two basic models will be discussed: 1) a sharp liquid-solid interface model corresponding to a mud-filled borehole in a homogeneous rock formation with sandstone like properties, 2) a velocity gradient model corresponding to a continuous change in properties between the mud-filled borehole and formation. which may resemble the combined effects of mud cake, formation, fracturing and invasion at the wall of the borehole. The displacement source in each case is computed from equation (3) with $\xi = 14.8 \times 10^8 \text{sec}^{-2}$ and $t_s = 0.064$ msec. The frequency content of the corresponding pressure pulse has a peak frequency (f_{peak}) of 15 kHz with an upper half-power frequency ($f_{+½}$) of 20 kHz. The formation and fluid properties used in these two cases are presented in Tables 1 and 2, respectively.

Figure 2 is a "snapshot" at 0.4 milliseconds after the source was triggered for the sharp interface model. Contours of vertical displacement amplitude are shown on a cross-section through the borehole. The compressional and shear head waves and the Stoneley and pseudo-Rayleigh waves can be identified. This type of plot shows the interactions in the rock and is a useful aid in identifying effects particularly when depth dependent borehole parameters are used. The vertical displacement amplitude time series corresponding to a receiver at 2.2 m below the source on the axis of symmetry is shown in Figure 3. The main features of a borehole acoustic log can be identified.

Figure 4 is a "snapshot" at 0.4 milliseconds after the source was triggered for the velocity gradient model. The key features are indicated. The vertical displacement amplitude time series corresponding to a receiver at 2.2 m below the source is shown in Figure 5. The first arrival in this case is a "diving wave" in the gradient and has a larger amplitude than the pure head wave in Figure 3. This effect was described by Helmberger (1968) for marine refraction profiles. The later phases in the wave train also differ significantly from the sharp interface case. A complete analysis of these arrivals will require further study.

Problems appear in both models after the Stoneley/pseudo-Rayleigh (or guided) wave packet. In the sharp interface case a high-frequency honey-comb pattern is evident near the source (Figure 2). The high frequency nature of this energy suggests that it is not real but a result of numerical noise. This problem has been solved since the figure was generated.

In the continuous gradient model there is a low frequency drift after the guided wave packet which appears to be a consequence of numerical instability. This problem was encountered in marine refraction applications and can be improved by finer grid meshes which unfortunately increase the costs of the seismograms considerably. Alternate solutions are under investigation.

Comparison between Finite Difference and Discrete Wavenumber Synthetic Microseismograms

To check the results from the Finite Difference Method (FD), it is necessary to compare them with results from a well established technique like the Discrete Wavenumber Summation Method (DW) (Cheng and Toksöz, 1981). The second order sharp interface model shown previously will be used, with the pressure response (different from the vertical displacement shown in Figures 2, 3, 4 and 5) in the center of the borehole presented as a function of time. The synthetic microseismograms from the discrete wavenumber summing will be presented for comparison.

As pointed out by several authors (Kelly *et al.*, 1976; Alford *et al.*, 1974; Alterman & Loewenthal, 1972; Stephen, 1983), the Finite Difference Method is very sensitive to the grid and time step size, distance to the absorbing boundary, and that the sharp interface solution will depend on the order of the Taylor series approximation. Different synthetic seismograms will be presented to illustrate how each different change may affect the final solution. On the other hand, the discrete wavenumber method is known to be exact (Bouchon and Aki, 1977); the only errors involved are those associated with the numerical evaluations of the modified Bessel functions of complex arguments. This type of numerical error is well understood and controlled.

In Figure 6a the synthetic seismogram calculated by the Discrete Wavenumber Method is presented. The formation and fluid properties are identical to those used in Figure 2. The radius of the borehole is 0.1m and the center frequency of the source is 15 kHz with a bandwidth of 5 kHz. The P and S wave arrivals, as well as the guided waves packet, can easily be identified. It is important to note that in this and subsequent comparisons, the DW solution will be shown in the upper halves of the figures, while the corresponding FD solution will be shown in the lower halves.

In Figure 6b we present the corresponding synthetic seismogram calculated using the Finite Difference Method. There is a very close match of the two waveforms; the P wave trains are almost identical, the S wave arrivals are also well matched, and there is a general agreement between the two microseismograms, including the pseudo-Rayleigh and Stoneley wave packet. There are some phasing differences in two microseismograms in the guided wave packet. In the tail end of the FD microseismogram there is some ringing that is absent from the DW microseismogram. This is believed to be due to the absence of attenuation in our model and the source generates reverberations in the liquid that travel with fluid velocity and are registered late in the record. In general, the overall agreement between the two methods is quite good.

Figure 7 shows the effect of reducing the time step. In the previous figure, the time step was taken to be as large as allowable in equation (5). In this figure the time step was reduced to half of the previous value. The two figures are identical except for the slight amplitude difference in the last cycle of the guided wave packet. It appears that the largest allowable time step is adequate in the generation of synthetic microseismograms. In fact, the largest allowable time step may be preferred in order to minimize the effects of grid dispersion (Alford *et al.*, 1974).

In Figure 8, the center frequency of the source is lowered to 10.6 kHz. There is an excellent match between the two microseismograms, with the only difference being a slight arrival time difference in the Stoneley wave pulses at about 1.35 msec.

It is clear from Figures 6 and 8 that the frequency content of the signal is very important in the resolution of the synthetic seismogram. The frequency content affects the choice of both the grid size and the time step in the FD solution. The time step is related to the grid size through equation (5), and the grid size is generally defined by:

$$\Delta x = \frac{V_{\min}}{10 f_{\max}} \tag{19}$$

The number 10 in the denominator represents the number of grid points per wavelength of the shortest wavelength body wave. In the case of a fluid filled borehole one must deal with not only P and S wave velocities but also pseudo-Rayleigh and Stoneley waves which propagate with velocities lower than the fluid velocity. The estimation of grid size in equation (19) must be changed accordingly. A factor of 0.8 is used in this study to reduce the smallest velocity in the system (α_f or β) for the grid size calculations.

Another consideration in the borehole problem is the maximum frequency $f_{\max}$ used in equation (19). Normally $f_{\max}$ is taken to be the upper-half-power frequency of the source. This frequency is used to generate the FD solutions shown in Figures 2, 6 and 7. In the borehole case, however, this frequency is not always adequate. Figure 9a shows the frequency spectrum of the DW synthetic microseismogram shown in Figure 6a. Although the source used in Figure 6 has an upper-half-power frequency at 20 kHz, there is significant energy at about 23 kHz. This is due to the excitation of the second mode of the pseudo-Rayleigh wave (Cheng and Toksöz, 1981; Paillet, 1980). The grid size used to calculate the waveform in Figure 6b gives a number of grid points per wavelength that is less than 10. This is reflected in the phasing difference in the pseudo-Rayleigh wave packets between the FD and DW synthetic microseismograms shown in Figure 6. For comparison, the frequency spectrum for the DW synthetic in Figure 8a is shown in Figure 9b. The higher mode of the pseudo-Rayleigh wave is clearly not excited at this lower frequency, and the grid spacing used is adequate.

Figure 10 shows the comparison results at an intermediate frequency (center frequency of 12.33 kHz). The similarity between the FD and DW solutions is better than the higher frequency solution shown in Figure 6 but not as good as the lower frequency solution shown in Figure 8. This is a confirmation of the frequency effect of the higher modes. Owing to the high cost of generating synthetic microseismograms in a model with many finely layered annuli using the discrete wavenumber summation method, no comparison between the heterogeneous formulation and the discrete wavenumber summation method has been made.

CONCLUSIONS

Synthetic acoustic logs which demonstrate the salient features of observed logs can be generated by the finite difference method using appropriate

formulations. The results we have shown are preliminary, and more comparisons between the finite difference results and those from the discrete wavenumber summation in simple formations are needed. Further work falls in three categories:

(1) Fine tuning the finite difference formulations; this includes eliminating the late arrival noise (sharp interface case) and instability (continuous gradient case).

(2) Further studies of the interaction of the guided waves with the sharp interface formulation. This is important in understanding the properties of the guided waves in a more complex formation.

(3) Applying the finite difference method to vertically varying borehole models to investigate the effects, in a forward approach, of varying borehole diameter and variable lithology between the source and receiver.

TABLES

Table 1: Parameters used for the Sharp Interface Formulation

SHARP LIQUID-SOLID INTERFACE	
0.0m	0.1m
α= 1.8 Km/sec β= 0.0 Km/sec ρ= 1.2 gm/cc	α= 4.0 Km/sec β= 2.3 Km/sec ρ= 2.3 gm/cc
MUD	SANDSTONE

Table 2: Parameters used for the Heterogeneous Formulation

LIQUID-SOLID INTERFACE		
0.0 m	0.1 m	0.2 m
α= 1.8 Km/sec β= 0.0 Km/sec ρ= 1.2 gm/cc	ZONE OF LINEAR GRADIENT	α= 4.0 Km/sec β= 2.3 Km/sec ρ= 2.3 gm/cc
MUD	--->	SANDSTONE

APPENDIX

The Source

The source is a compressional point source in the water column. The time dependence of the potential of the source is assumed to be:

$$\varphi(r,z,t) = -2\xi T e^{-\xi T^2}, \qquad T = (t - t_s + \frac{R}{\alpha}) \tag{A.1}$$

and the Fourier transform of the potential is*:

$$\Phi(r,z,\omega) = -i\pi^{1/2}\xi^{-1/2}\omega e^{-\omega^2/4\xi} e^{i\omega(t_s - R/\alpha)}, \tag{A.2}$$

where ξ is a pulsewidth parameter
t_s is a time shift parameter
$R = (r^2+z^2)^{1/2}$ is the distance between the source and the observation point
α is the compressional wave velocity in the region around the source.
and ω is angular frequency.

Since the displacement $\vec{u}$ is the gradient of the potential, the time dependence of the displacement is:

$$\vec{u}(r,z,t) = \begin{pmatrix} \frac{r}{R} \\ \frac{z}{R} \end{pmatrix} \frac{-2\xi}{\alpha}[1 - 2\xi T^2]\, e^{-\xi T^2} \tag{A.3}$$

and the Fourier transform of the displacement is:

$$\vec{u}(r,z,\omega) = \begin{pmatrix} \frac{r}{R} \\ \frac{z}{R} \end{pmatrix} \frac{\omega^2}{\alpha}\, \pi^{1/2}\, \xi^{-1/2}\, e^{-\omega^2/4\xi}\, e^{i\omega(t_s - R/\alpha)} \tag{A.4}$$

Similarly, the time and frequency dependence of the pressure field can be calculated ($p = \alpha^2\rho\nabla\cdot\vec{u} = \alpha^2\rho\nabla^2\varphi = \alpha^2\rho\frac{\partial^2\varphi}{\partial t^2}$):

$$p(r,x,t) = \alpha^2\rho 4\xi^2[3T - 2\xi T^3]\, e^{-\xi T^2}, \qquad T = (t - t_s + \frac{R}{\alpha}) \tag{A.5}$$

---

*The Fourier transform is defined by:

$$F(\omega) = \int_{-\infty}^{\infty} f(t) e^{-i\omega t}\, dt \qquad f(t) = \frac{1}{2\pi}\int_{-\infty}^{\infty} F(\omega) e^{+i\omega t}\, d\omega.$$

$$p(r,z,\omega) = \alpha^2 \rho i \left(\frac{\pi}{\xi}\right)^{1/2} \omega^3 \, e^{-\omega^2/4\xi} \, e^{i\omega(t_s - R/\alpha)} \qquad \text{(A.6)}$$

The time shift parameter, t_s, is adjusted automatically by the program to give a vanishingly small starting value for the displacement at the closest range (R_{min}) to the source. The program sets

$$t_s = -\frac{R_{min}}{\alpha} + \sqrt{\frac{14}{\xi}}$$

which yields a value of approximately 10^{-6} for $e^{-\xi(t - t_s + R/\alpha)}$ at $t = 0$. This starts the finite difference calculations sufficiently smoothly for stable results. Similarly, there is no point in continuing the source after it has become less than approximately 10^{-6} at the maximum range R_{max}. The program ceases to calculate the source and replaces it with zero when t exceeds t_{max}, given by

$$t_{max} = t_s + \frac{R_{max}}{\alpha} + \sqrt{\frac{14}{\xi}}$$

The peak frequency and bandwidth are determined from the pulsewidth parameter, ξ. For a pressure source, from equation (A.6), the peak frequency is given by

$$f_{peak} = 0.39\sqrt{\xi}$$

with the upper-half-power and the lower-half-power frequencies given by $0.528\xi^{1/2}$ and $0.266\xi^{1/2}$, respectively. The bandwidth, defined by the distance between the two half-power points, is given by $0.262\xi^{1/2}$.

REFERENCES

Aki, K. and Richards, P.G., 1980, Quantitative Seismology: Theory and Methods, W.W. Freeman and Company, San Francisco.

Alford, R.M., Kelly, K.R. and Boore, D.M., 1974, Accuracy of finite-difference modeling of the acoustic wave equation: Geophysics, v.39, p.834-842.

Alterman, Z.S. and Karal F.C., 1968, Propagation of elastic waves in layered media by finite difference methods: Bull. Seism. Soc. Am., v.58, p.367-398.

Alterman, Z. and Loewenthal, D., 1972, Computer generated seismograms: In: Methods in Computational Physics, v.12: Bolt, B.A., Ed., Academic Press, New York, p.35-164.

Bamberger, A., Chavent, G. and Lailly, P., 1980, Etudes de schémas numériques pour les équations de l'élastodynamique linéaire: Rapports de Recherce, v.41, INRIA, B.P. 105, 78150 Le Chesnay, France.

Biot, M.A., 1952, Propagation of elastic waves in a cylindrical bore containing a fluid: J. Appl. Phys., v.23, p.997-1005.

Boore, D.M., 1972, Finite difference methods for seismic waves: In: Methods in Computational Physics, v. 11: Bolt, B.A., Ed., Academic Press, New York, p.1-37.

Bouchon, M., and Aki K., 1977, Discrete wave-number representation of seismic-source wave fields: Bull. Seism. Soc. Am., v.67, p.259-277.

Cheng, C.H. and Toksöz, M.N., 1981, Elastic wave propagation in a fluid-filled borehole and synthetic acoustic logs: Geophysics, v.46, p.1042-1053.

Clayton, R. and Engquist, B., 1977, Absorbing boundary conditions for acoustic and elastic wave equations: Bull. Seism. Soc. Am., v.67, p.1529-1540.

Emerman, S.H. and Stephen, R.A., 1983, Comment on, "Absorbing boundary conditions for acoustic and elastic wave equations," by R. Clayton and B. Engquist: Bull. Seism. Soc. Am., in press.

Fuyuki, M. and Matsumoto Y., 1980, Finite difference analysis of Rayleigh wave scattering at a trench: Bull. Seism. Soc. Am., v.67, p.1529-1540.

Helmberger, D.V., 1968, The crust-mantle transition in the Bering Sea: Bull. Seism. Soc. Am., v.58, p.179-214.

Kelly, K.R., Ward, R.W., Treitel, S., and Alford, R.M., 1976, Synthetic seismograms: A finite difference approach: Geophysics, v.41, p.2-27.

Paillet, F.L., 1980, Acoustic propagation in the vicinity of fractures which intersect a fluid-filled borehole: paper presented at 21st Annual Logging Symposium, Lafayette, LA.

Stephen, R.A., 1983, A comparison of finite difference and reflectivity seismograms for marine models: Geophys. J.R. Astr. Soc., v.72, p.39-57.

Tsang, L. and Rader D., 1979, Numerical evaluation of the transient acoustic waveform due to a point source in a fluid-filled borehole: Geophysics, v.44, p.1706-1720.

Ungar, A. and Ilan, A., 1977, Propagation of elastic waves in vertically inhomogeneous media: J. Geophys., v.43, p.33-40.

White, J.E., 1962, Elastic waves along a cylindrical bore; Geophysics, v.27, p.327-333.

White, J.E. and Zechman R.E., 1968, Computed response of an acoustic logging tool, Geophysics, v.33, p.302-310.

Zienkiewicz, O.C., 1977, The Finite Element Method. McGraw-Hill, London.

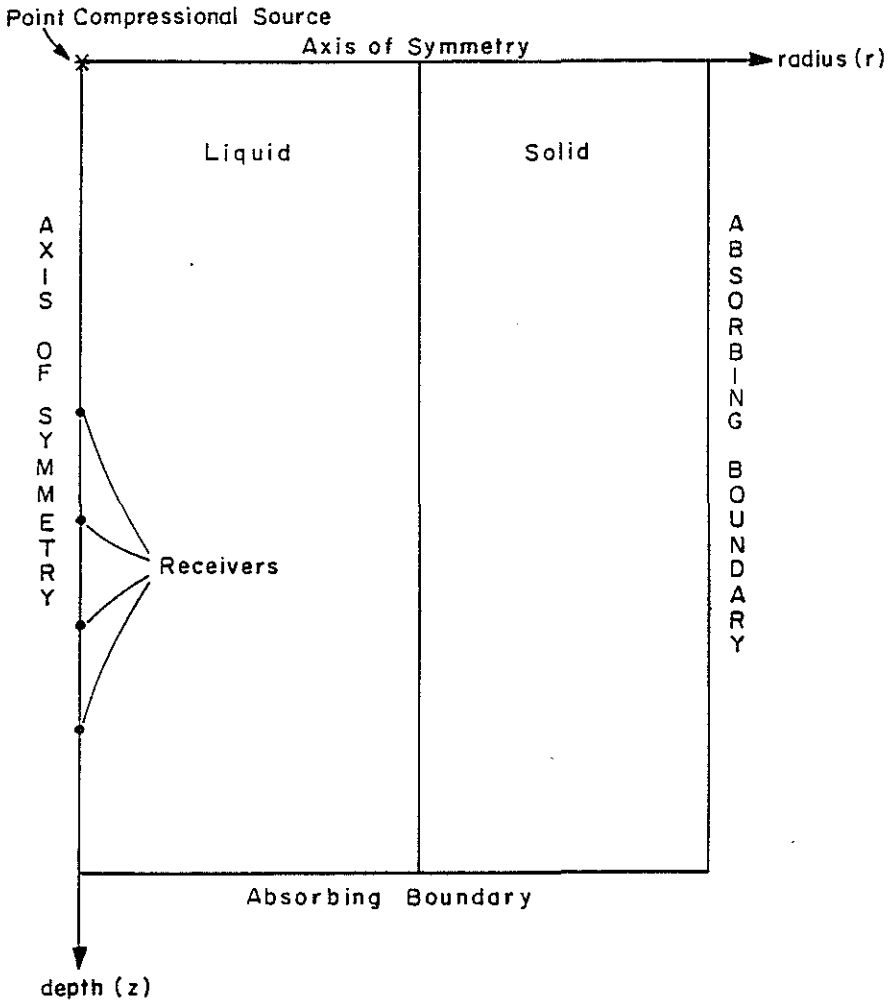

Figure 1. Outline of the geometry used for finite difference synthetic acoustic logs. Co-ordinates and types of boundaries are shown.

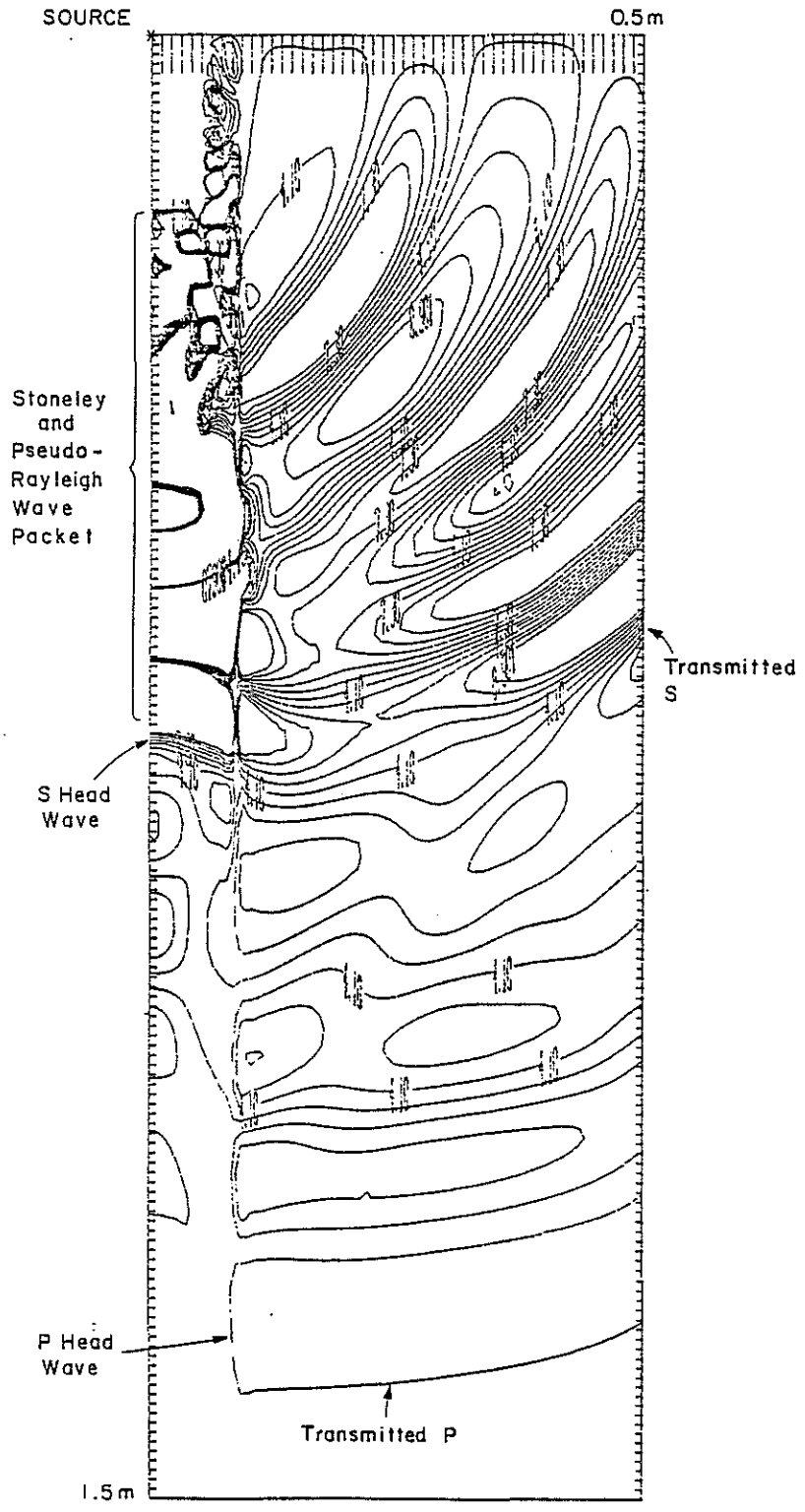

Figure 2. Snapshot of the borehole response 0.4 milliseconds after the source was triggered for a sharp liquid-solid interface model. The Key wave types are identified. This plot shows contours of vertical displacement amplitude so that shear waves can be identified in the formation.

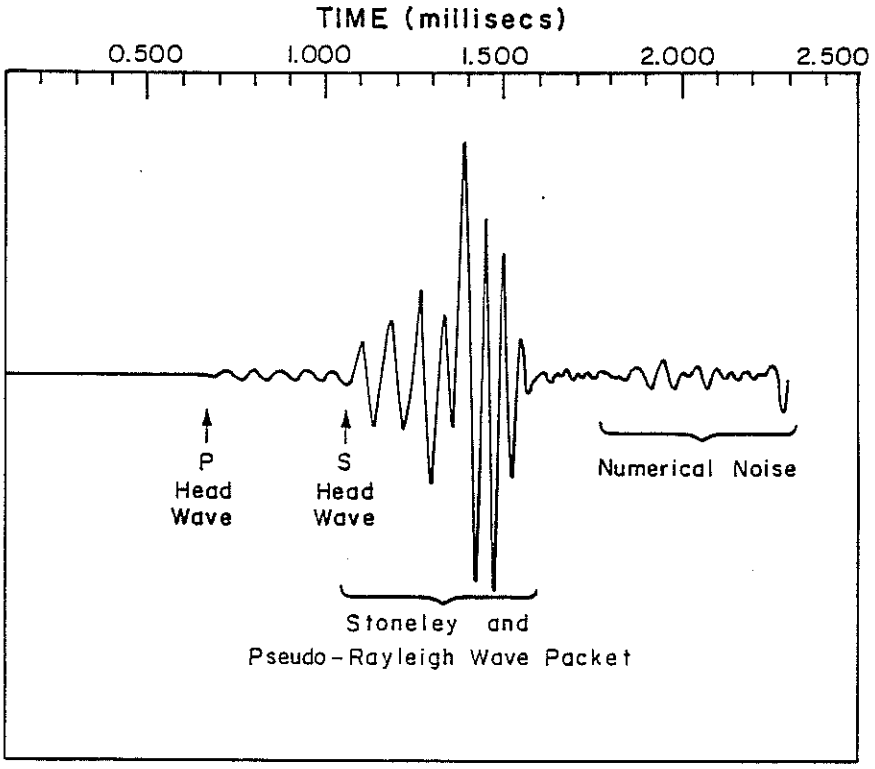

Figure 3. The vertical displacement time series observed at 2.2 m directly below the source for the sharp liquid-solid interface model. Key wave types are identified.

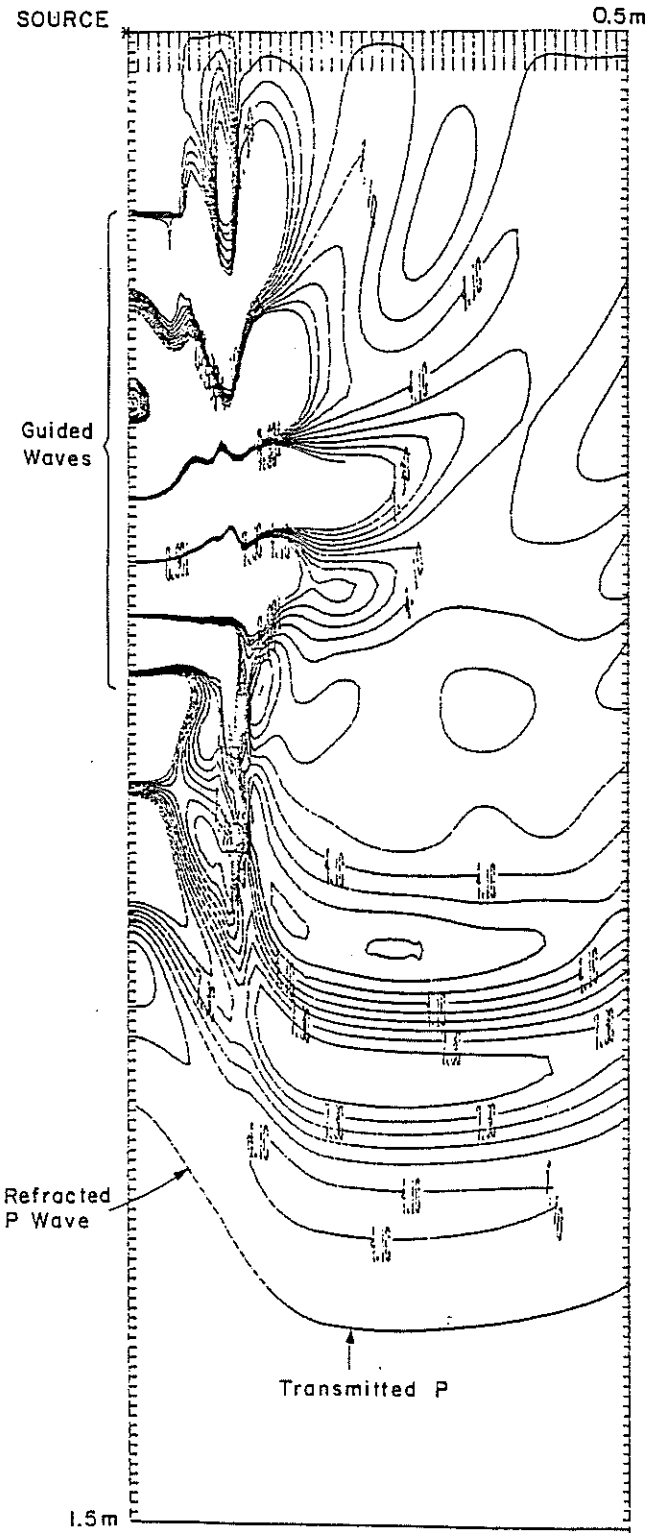

Figure 4. Snapshot at 0.4 millisecond for a model with a linear gradient between the borehole fluid properties and the rock. Vertical displacement amplitude has been contoured.

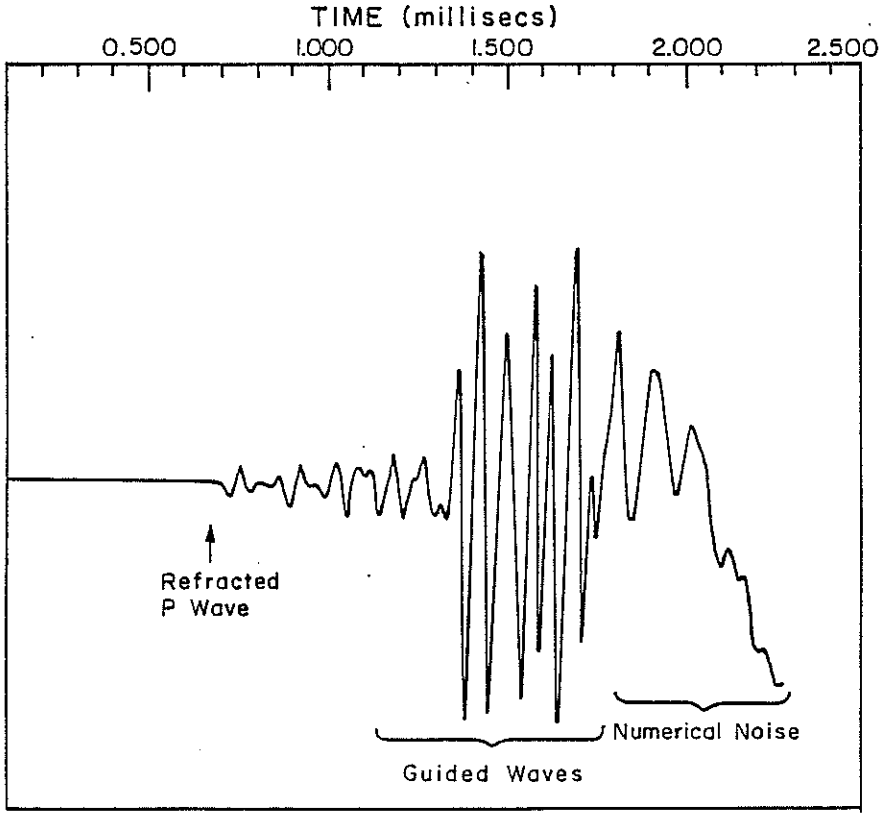

Figure 5. The time series observed at 2.2 m below the source for the linear gradient model. Note that the first P wave arrival, the refracted or diving P wave, has a larger amplitude than the P head wave observed at a sharp interface. Shear wave conversion is less pronounced for the gradient case and the refracted shear wave, if it is present,is difficult to identify. The guided wave packet, corresponding to the Stonely/pseudo-Rayleigh wave packet for the sharp interface case, is still present, and, indeed, appears to have larger amplitude arrivals over a longer period. The sources for the two models are identical.

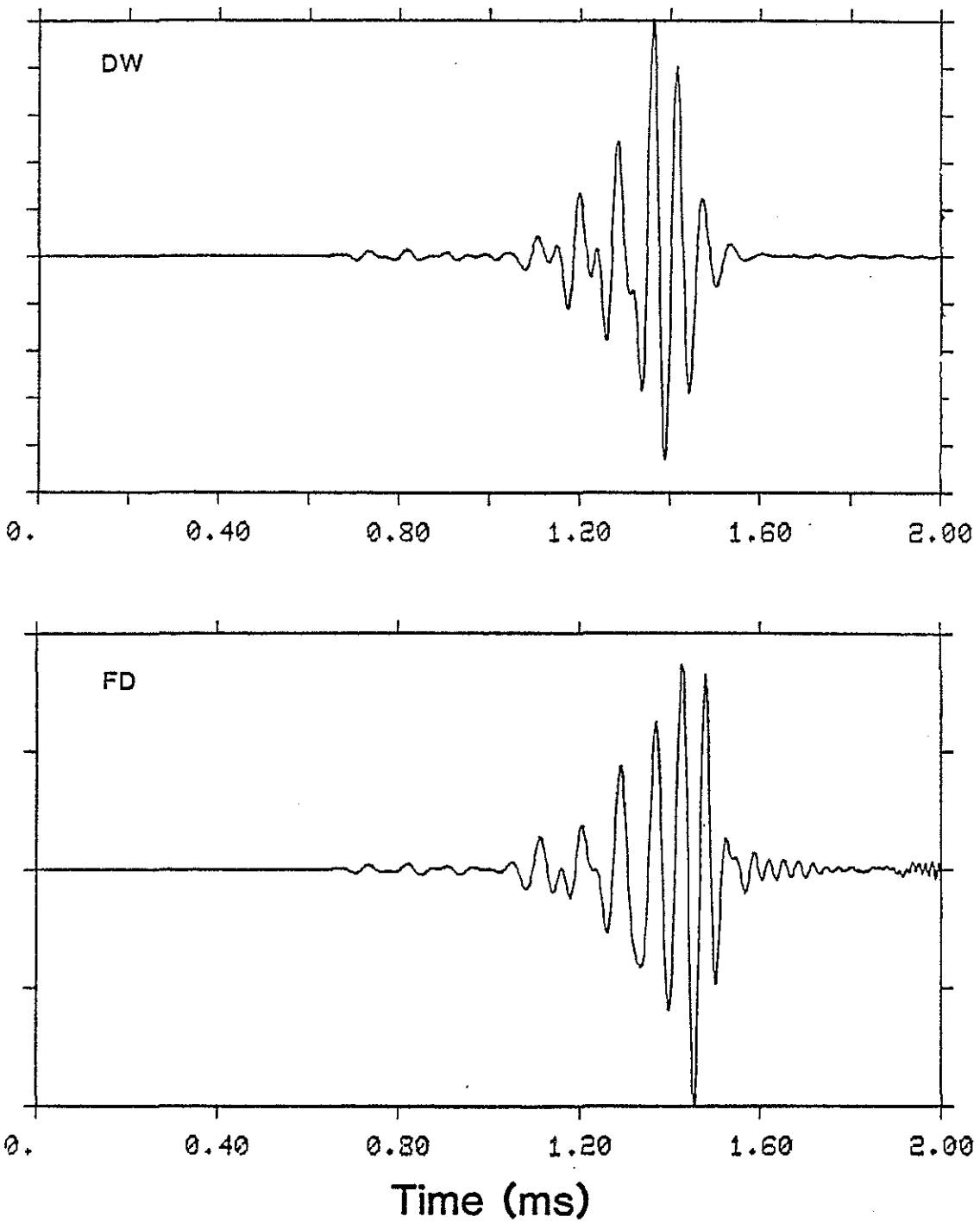

Figure 6. (a) Discrete wavenumber (DW), and (b) finite difference (FD) synthetic seismogram (DW) at 2.2 m. The center frequency of the source is 15 kHz.

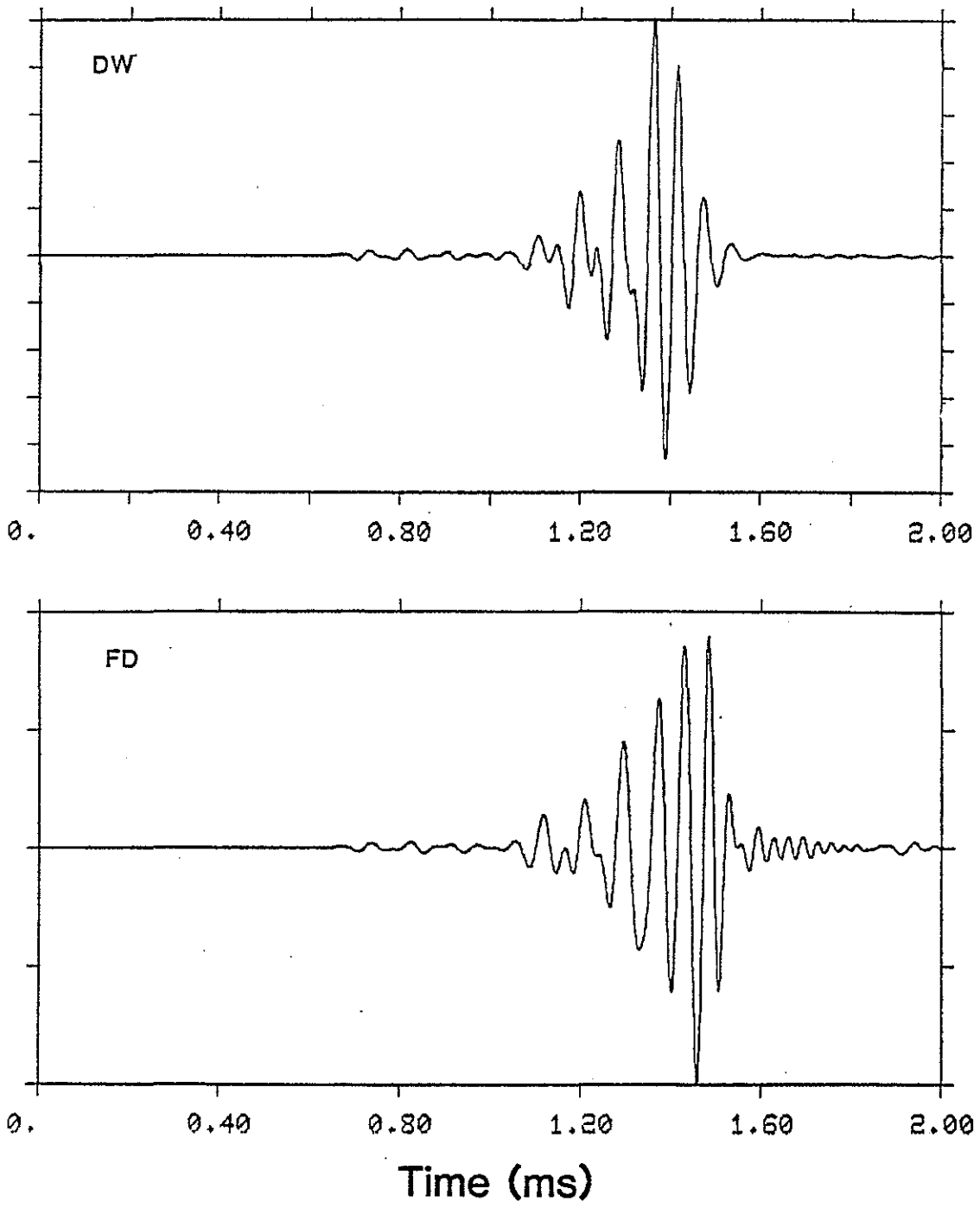

Figure 7. (a) Discrete wavenumber (DW), and (b) finite difference (FD) synthetic seismogram (DW) at 2.2 m. The center frequency of the source is 15 kHz. The time step used in the finite difference solution here is half that used in Figure 6b

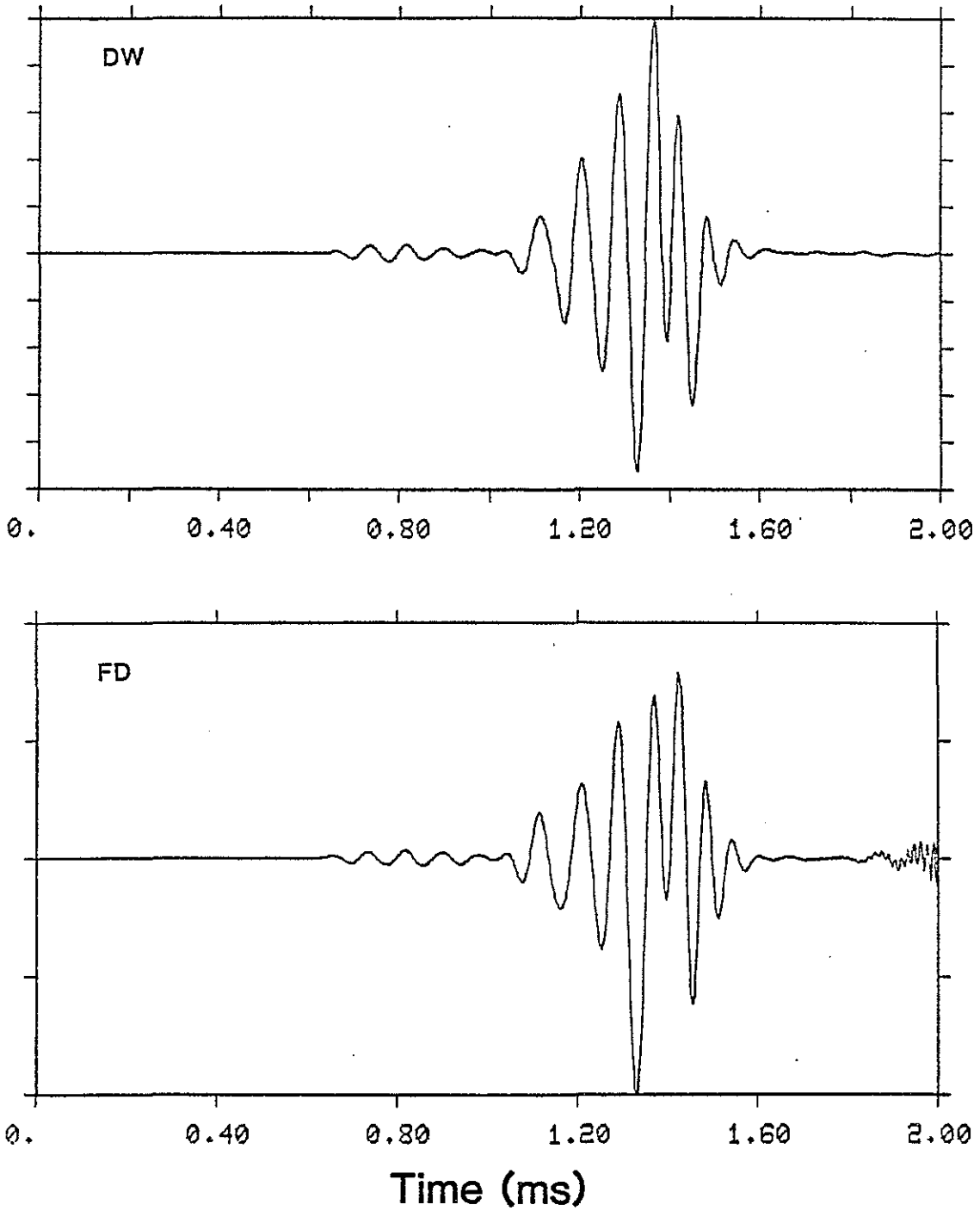

Figure 8. (a) Discrete wavenumber (DW), and (b) finite difference (FD) synthetic seismogram (DW) at 2.2 m. The center frequency of the source is 10.6 kHz.

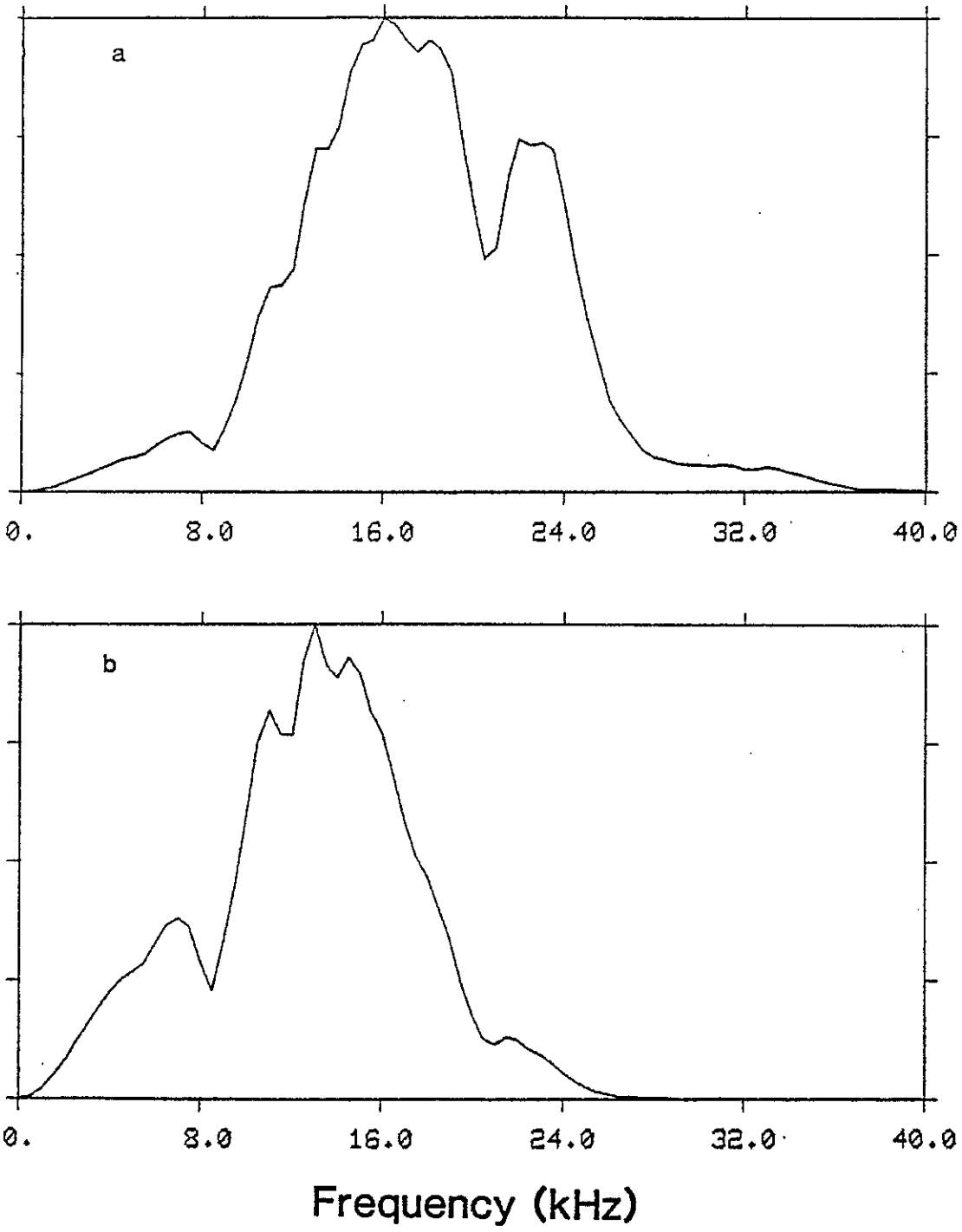

Figure 9. (a) Frequency Spectrum of the DW synthetic seismogram in Figure 6a. Notice the energy at about 23kHz. (b) Frequency Spectrum of the DW synthetic seismogram in Figure 8a.

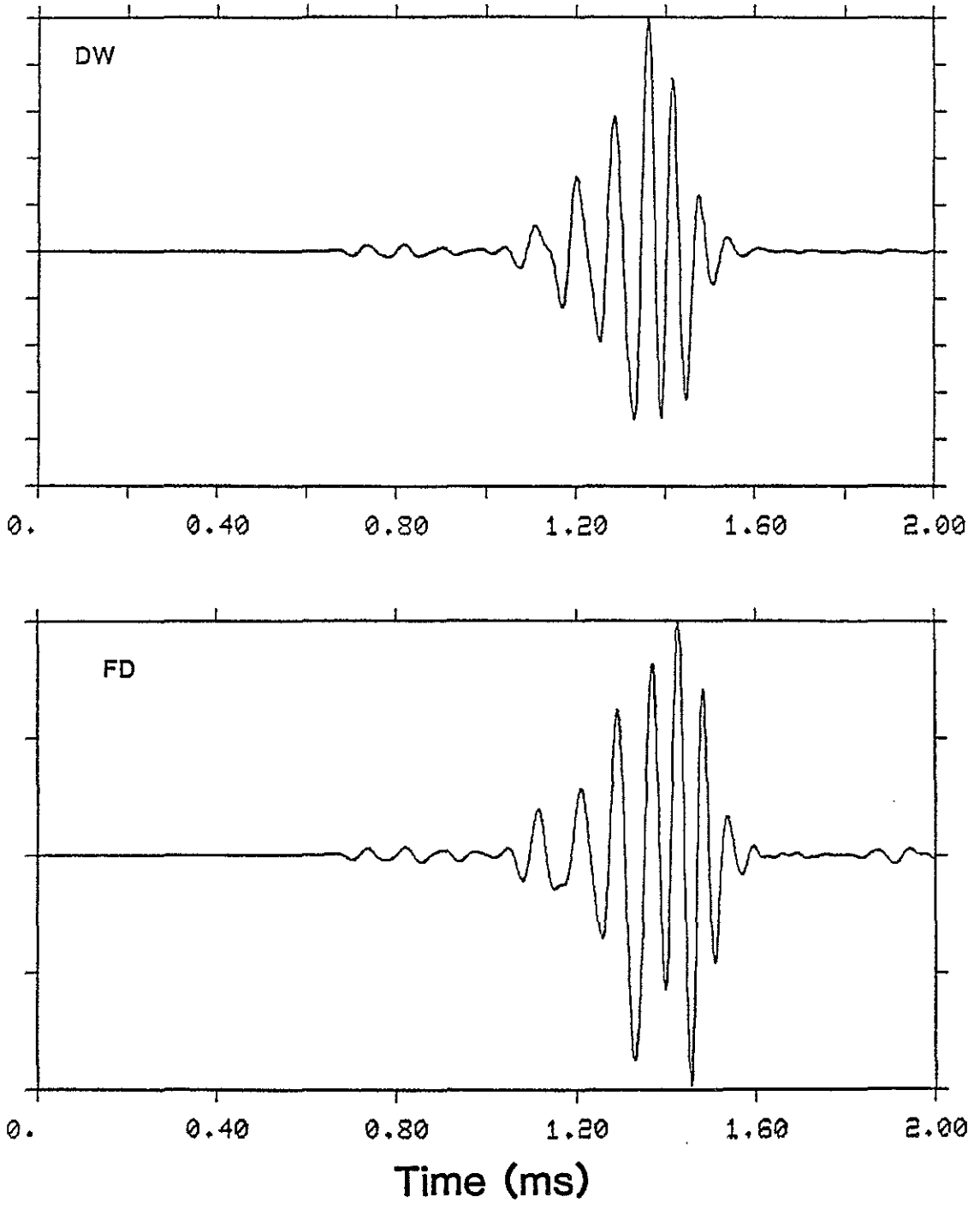

Figure 10. (a) Discrete wavenumber (DW), and (b) finite difference (FD) synthetic seismogram (DW) at 2.2 m. The center frequency of the source is 12.33 kHz.